Bull Volcanol (2001) 63:238–251
DOI 10.1007/s004450100138

RESEARCH ARTICLE

Gerardo J. Aguirre-Díaz

Recurrent magma mingling in successive ignimbrites from Amealco caldera, central Mexico

Received: 8 April 1999 / Accepted: 7 February 2001 / Published online: 17 May 2001

Abstract The Amealco Tuff is a widespread (>2880 km^2), trachyandesitic to rhyolitic pyroclastic deposit in the central Mexican Volcanic Belt that was erupted from the Amealco caldera at 4.7±0.1 Ma. It includes three major ignimbrites, each showing complex mingling of pumice fragments and matrix glass with andesitic to rhyolitic compositions. The different glasses are well mingled throughout each of the pyroclastic-flow deposits. Mingling of glasses may have occurred just before and during the explosive eruptions that produced the pyroclastic flows, as the distinct melts had insufficient time to homogenize. Mingling of glasses is evident in each of the three separate major ignimbrites of the Amealco Tuff; thus, the processes that caused it were repetitive. It is infered that the repetitive mingling of melts was due to repeated mafic magma inputs to an evolved magma chamber.

Keywords Ignimbrite · Caldera · Magma mingling · Glass · Amealco, Mexico

Introduction

There are several reports in the literature of ignimbrites containing distinct glass compositions dispersed throughout the deposit (e.g., Williams 1952; Martin and Lewis 1963; Walker and Skelhorn 1966; Fries et al. 1977; Mahood et al. 1985; Pallister et al. 1996; Streck and Grunder 1997, 1999). In this work I present a case in central Mexico of mingling of glasses with distinct compositions within large-volume ignimbrites. The ignimbrites are part of the Amealco Tuff which erupted from the Amealco caldera in the central sector of the Mexican Volcanic Belt (Fig. 1). The glass mingling in the Amealco ignimbrites was recognized by Fries et al. (1977) who described the nature of the southern distal facies of these deposits. Similar examples of pyroclastic flows containing ranges of pumice and glass compositions at the same stratigraphic level, and even in the same thin section, are reported by Lipman (1967), Briggs et al. (1993), Orsi et al. (1995), Mandeville et al. (1996), and Streck and Grunder (1997). The case of Amealco caldera's ignimbrites offered here is unusual in showing magma mingling in three successive eruptions.

We use the terms mixing and mingling as proposed by Bardintzeff (1992). In magma mixing, melts are mostly hybrid and the identities of the end members are not obvious or were not preserved in the rock, whereas in magma mingling, end-member components are easily recognizable on megascopic scales (e.g., banded pumices). We focus on the field characteristics and the glass compositions obtained from whole-rock analyses of pumices and from microprobe analyses in small pumices and glass shards. Based on this evidence, we then discuss a model for the occurrence of these ignimbrites.

Editorial responsibility: W. Hildreth

G.J. Aguirre-Díaz (✉)
Department of Geological Sciences of the
University of Texas at Austin, Austin, Texas, USA
e-mail: ger@unicit.unam.mx

Present address:
G. J. Aguirre-Díaz, Unidad de Investigación
en Ciencias de la Tierra, Instituto de Geología, UNAM, Juriquilla,
Querétaro, México 76230

Geologic setting and field characteristics

The Amealco Tuff is a >77-km^3 (dense rock equivalent, DRE), widespread pyroclastic deposit (Fig. 1), predominantly of trachyandesitic to trachydacitic composition (Aguirre-Díaz 1993, 1996), but it includes volumetrically minor andesite and rhyolite. It was erupted from the Amealco caldera at 4.7±0.1 Ma within the Mexican Volcanic Belt, which has been related to subduction of the Cocos and Rivera oceanic plates beneath southern Mexico (Nixon 1982; Pardo and Suárez 1995). The Amealco Tuff includes four ignimbrites and interbedded pumice fallout, surge, and mud-flow deposits (Fig. 2). The ignimbrites are referred to (from oldest to youngest) as

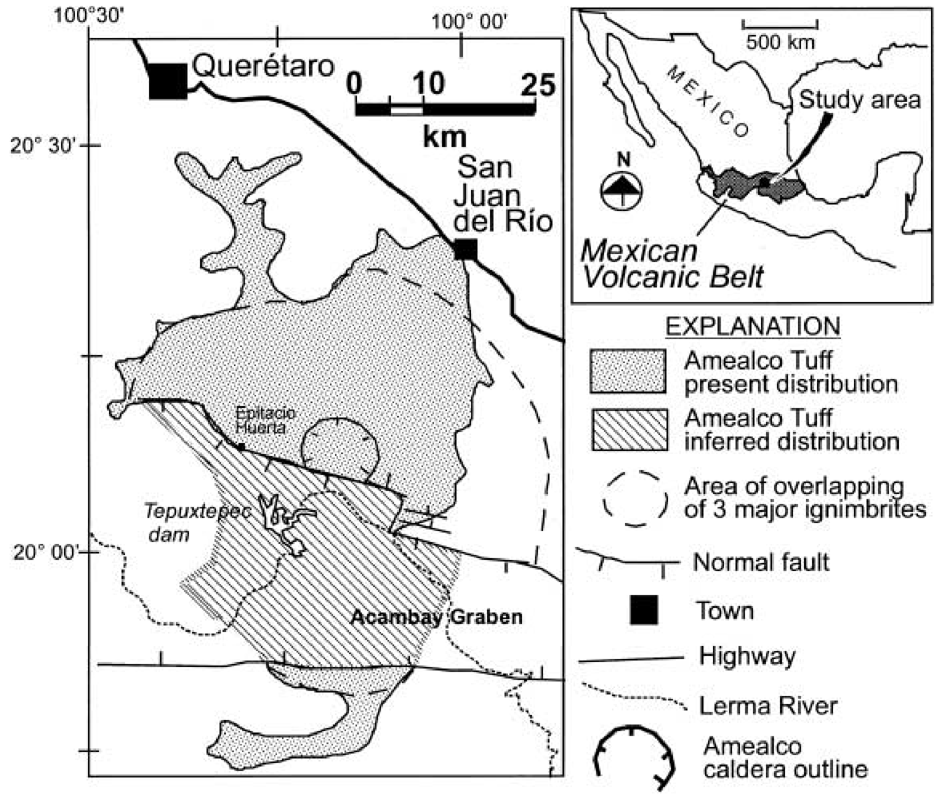

Fig. 1 Distribution of the Amealco Tuff and its source, the Amealco caldera. *Inset* shows the regional location of the study area and of the Mexican Volcanic Belt

Table 1 K–Ar ages of Amealco Tuff ignimbrites. *scc/g* standard cubic cm/g

Unit	Sample	Location		Material[a]	K (%)	Weight (g)	Ar $\times 10^{-6}$ scc/g	^{40}Ar[b] (%)	Age (Ma)	±1 σ[c] (Ma)	Assigned age[d] (Ma±1 σ)
		Lat. N	Long. W								
Amealco III	Am-12	20°16′35″	100°9′7″	Feldspar	0.46 0.46	0.301	0.082	13.1	4.55	0.40	4.68±0.10
Amealco II	Am-22	20°8′1″	100°18′8″	Glass	3.62 3.53 3.56 3.53	0.432 0.277	0.640 0.664	35.9 31.1	4.71	0.14	
Amealco I	Am-208	19°50′45″	100°11′15″	Glass	2.90 2.91 2.86	0.606 0.278	0.542 0.524	34.4 38.8	4.71	0.19	
Amealco I	Am-1	20°8′3″	100°18′10″	Glass	4.64 4.61 4.63	0.263	0.854	18.5	4.74	0.15	
	Am-1			Feldspar	0.53 0.53	0.316	0.094	19.9	4.54	0.28	

[a] Material used for K–Ar analysis
[b] Ar-40: radiogenic argon content of sample, in percent of total ^{40}Ar
[c] Error of age at one sigma
[d] Weighted mean of the different ages
$^{40}K/K=1.167\times10^{-4}$ moles/mole, $\lambda\varepsilon+\varepsilon=0.581\times10^{-10}$/year, $\lambda\beta=4.963\times10^{-10}$/year

Amealco Zero, Amealco I, Amealco II, and Amealco III. Amealco Zero is a minor local deposit with a DRE volume of 0.75 km^3. Amealcos I, II, and III are major ignimbrites, with DRE volumes of 8.7, 11.1, and 13.8 km^3, respectively. If we consider also the associated pyroclastic fall and surge deposits of Amealco Tuff (Fig. 2), the DRE volumes for each major ignimbrite cycle are 20.7, 32.3, and 24.0 km^3, respectively, for a minimum total of 77.8 km^3 (for details of volume estimations see Aguirre-Díaz 1993). Each of the three major ignimbrites is generally 3–10 m thick, with aspect ratios of the order of 0.0003 (the ratio of the average thickness to the maximum distance from the source of the ignimbrite). The three major ignimbrites are co-extensive for at least 30 km around the source (Fig. 1). Farther away, only one or two ignimbrites continued as far as 45 km from the

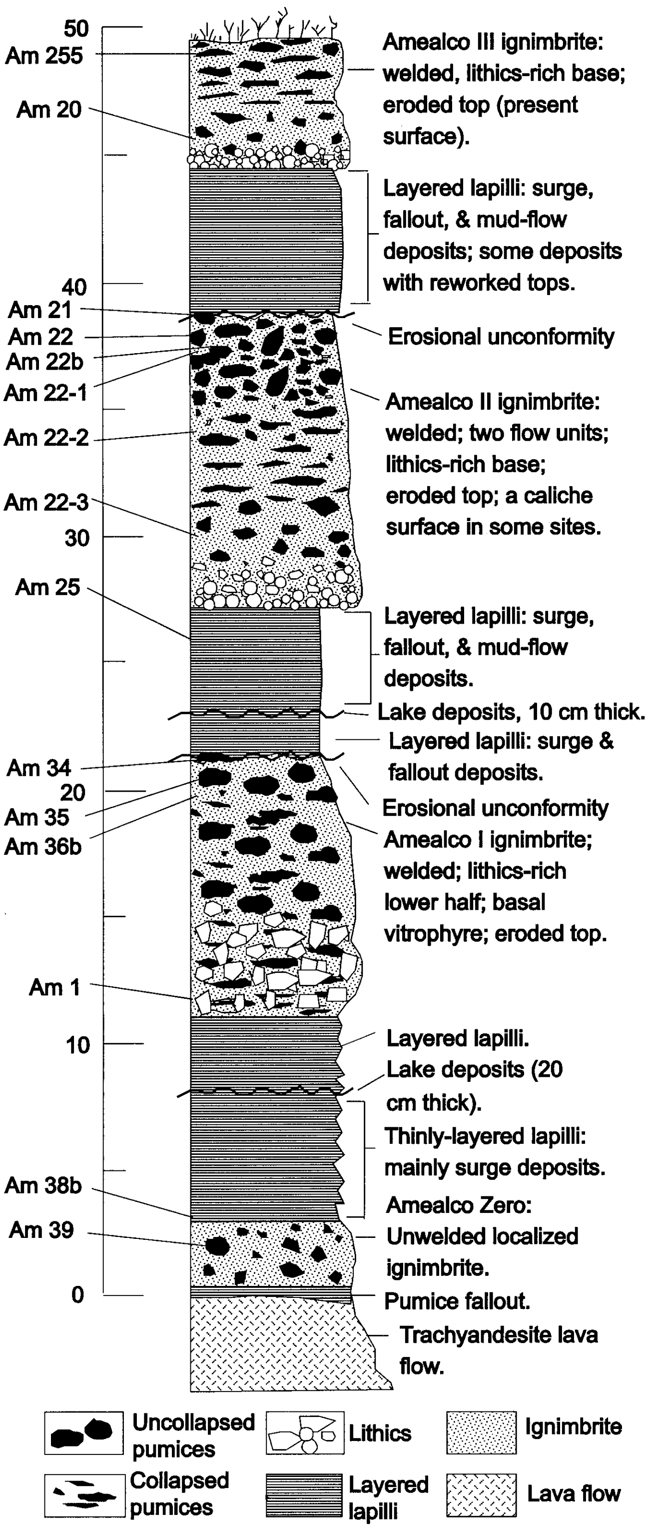

Fig. 2 Representative section of Amealco Tuff measured at Epitacio Huerta, 13 km west of the source (see Fig. 1). Section has been simplified for clarity. *Wavy thicker lines* indicate unconformities. *Numbers at the left side of column* are sample numbers (e.g., Am-22). *Scale at left* in meters

source. To the east, Amealco Tuff is covered by a younger felsic ignimbrite derived from another source, the Huichapan caldera, which is farther to the east, but deep canyons that cut through this capping ignimbrite exposed the Amealco Tuff as far as 30 km northeast of the Amealco caldera. Based on measured stratigraphic sections (Aguirre-Díaz 1993, 1996) and magneto-stratigraphic correlations (Aguirre-Díaz et al. 2000), it is usually possible to distinguish the isolated distal ignimbrites. The major ignimbrites are generally densely welded with vertical jointing (Fig. 3a). They are gray to dark gray, in some outcrops with red-orange tops due to vapor-phase oxidation.

Each major Amealco ignimbrite is separated from the overlying ignimbrite by erosional unconformities overlain by deposits that include lacustrine sediments, airfall and surge deposits, and paleosols; these indicate significant time gaps between ignimbrite eruptions. Five K–Ar ages on the Amealco Tuff range from 4.5 to 4.7 (Table 1), with a weighted mean of 4.7±0.1 Ma. The K–Ar determinations do not have the resolution necessary to establish age differences among the eruptions. ^{40}Ar–^{39}Ar ages on Amealco ignimbrite glasses were carried out in hope of getting better precision, but the results were more scattered than the K–Ar data, so I decided to reject the ^{40}Ar–^{39}Ar data.

Each of the three major ignimbrites shows a complex mingling of glass types in the form of pumice fragments and glass shards with distinct colors. Most glass is not devitrified, but it is slightly hydrated. Megascopically, pumice fragments can be black, and less commonly, white (Fig. 3b). Under the microscope, pumices and shards are dark brown, yellow, or colorless (black and white in Fig. 4a). The pumices of various colors are dispersed throughout each deposit apparently with no order (Fig. 3b), but in some outcrops there is evidence of vertical zoning, with rhyolitic glasses concentrated in the basal part and andesitic–dacitic glasses at the top. Most pumice fragments are homogeneous in color, although banded black and white clasts are ubiquitous (Fig. 4b). Black pumices predominate, making up to 40 vol.% of each ignimbrite, with the larger fragments, <40 cm in diameter, concentrated at the top of each ignimbrite. White or light-colored pumices make up less than 20 vol.% at the base of the deposits, and commonly less than 5 vol.% at the tops. Discrete white and black pumices deformed during welding and compaction (Fig. 4a); thus, the various discrete pumices are juvenile fragments and not accidental. White pumices are generally more compressed than the black pumices (Fig. 4a). During welding and compaction the different pumices behaved differently at the same welding temperature, with rhyolitic pumices becoming more flattened than the black ones. This was probably related to the differences in composition of the pumices. It takes detailed mineralogical and geochemical studies in glasses to know the rheology of glasses in ignimbrites, which are not intended here.

The mineralogy is the same in all three major Amealco ignimbrites and interbedding pyroclastic fall and surge deposits. The Amealco ignimbrites include plagioclase, 10–22 vol.%; hypersthene, 3–5 vol.%; augite, 1–3 vol.%; ilmenite, 1–2 vol.%; titanomagnetite, 1–3 vol.%; olivine, <1 vol.%, ±apatite±zircon. Crystal contents increase from Amealco I to Amealco II, to Amealco III, in proximal and distal facies (Fig. 5).

Fig. 3a, b Amealco Tuff ignimbrite showing distinct megascopic characteristics. **a** Cliff-forming Amealco II ignimbrite 25 km northeast of source; a densely welded deposit with vertical jointing and underlying plane-bedded surge deposits. Lithic-poor layer 2a (sensu Sparks et al. 1973) is observed at the base of the ignimbrite (poorly welded, light-gray layer beneath the darker, massive unit, layer 2b). For a detailed description of this section see Aguirre-Díaz (1996). **b** Amealco II ignimbrite with black and white pumice lumps, mostly as discrete fragments, in a dark-gray matrix. White pumices have rhyolite composition, and black pumices have andesite, trachyandesite, and trachydacite compositions. *Coin* is 2.5 cm in diameter

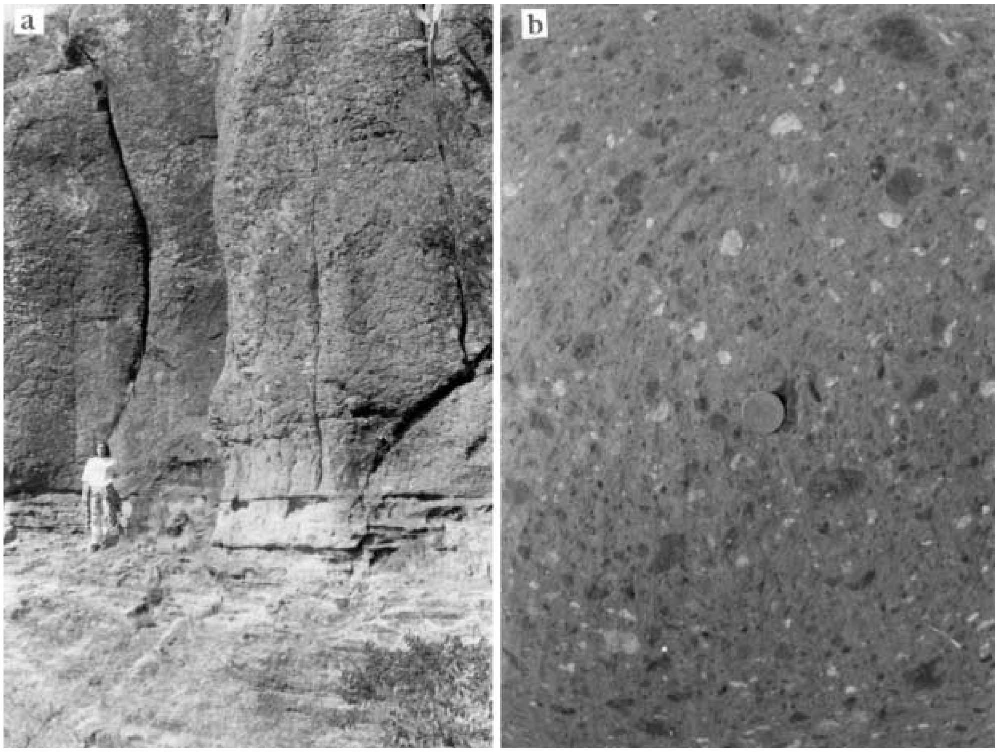

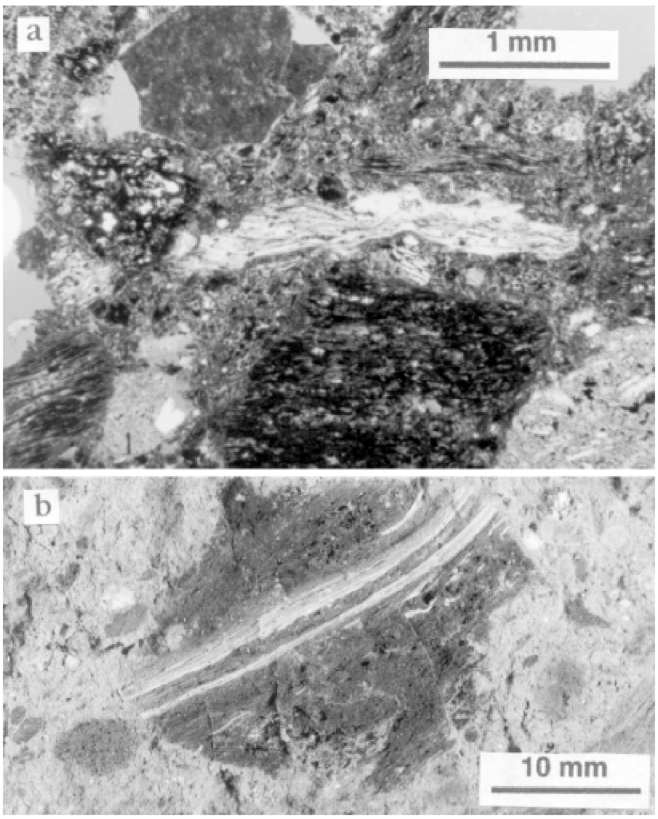

Fig. 4 **a** Photomicrograph of Amealco Tuff ignimbrite (transmitted light) showing compacted black (*lower center* and *lower left*) and white (*center*) pumices indicating that distinct, discrete glassy clasts behaved plastically during welding and compaction, and that both black and white pumices are therefore juvenile. **b** Cut slab of banded pumice in Amealco Tuff ignimbrite surrounded by discrete glassy clasts with different gray shades, each shade corresponding to a distinct composition (sample Am-243 of Table 4)

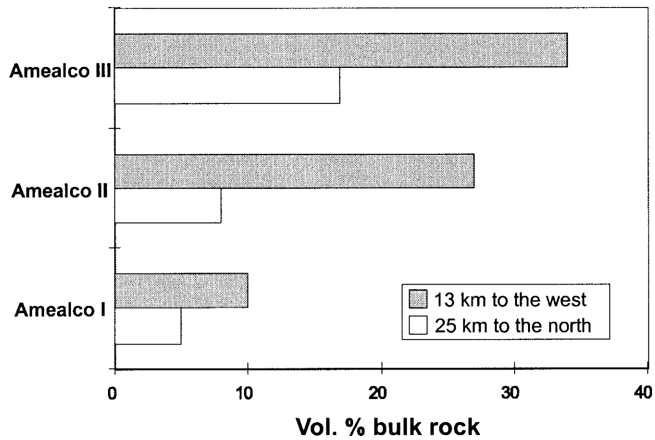

Fig. 5 Bulk tuff crystal volume percent in Amealco I, Amealco II, and Amealco III. Values are from two representative measured sections, one from proximal facies at 13 km to the west of the caldera center (Epitacio Huerta site), and the other from distal facies at 25 km to the north of the caldera center. In both the proximal and the distal ignimbrites there is a progressive increase of crystal content from Amealco I to Amealco III. Modal values are in Aguirre-Díaz (1993)

Analytical methods

Pumices were analyzed by Inductively Coupled Plasma Atomic Emission Spectrometry (ICP-AES), by Inductively Coupled Plasma Mass Spectrometry (ICP-MS), and a few of them by X-ray fluorescence (XRF). Pumice samples, generally larger than 5 cm in diameter, were crushed and ground using an alumina ceramic container and a shatter box to obtain a homogeneous powder that passed the 200-mesh screen. Sample preparation for rare earth elements analyzed by ICP-AES in-

Table 2 Whole-rock chemical analyses of pumices in Amealco Tuff ignimbrites. *n.d.* Not determined

Sample	Am-39a*	Am-39b	Am-258w*	Am-258b	Am-35	Am-34	Am-73	Am-22	Am-75	Am-230	Am-21	Am-255	Am-256	Am-99	Am-243	Am-177	Es1N*	Es1B*	Es2N*	Es2B*	Es3N*	Es3B*	Es4N*	Es4B*
Ignimbrite	Zero	Zero	I	I	I	I	I	II	II	II	II	III	III	III	III	III	III	III	III	III	III	III	III	III
SiO_2	55.10	58.84	73.80	60.23	59.51	60.77	61.67	64.38	62.01	60.08	60.83	63.85	61.14	61.23	57.00	63.80	60.85	66.71	61.24	66.84	61.83	68.03	62.56	68.30
TiO_2	1.23	1.20	0.18	0.87	1.21	1.03	0.76	0.81	1.01	1.00	1.05	0.71	0.82	0.97	1.22	0.77	0.93	0.22	0.94	0.25	0.94	0.27	0.85	0.26
Al_2O_3	16.60	15.95	14.20	14.32	15.97	15.81	15.72	15.46	16.12	14.83	15.72	15.25	14.42	15.76	16.31	15.42	14.99	13.93	15.21	14.35	15.03	14.48	14.12	13.99
Fe_2O_3	3.04	3.53	0.35	2.19	3.21	2.81	2.54	1.79	3.51	3.52	2.40	2.58	2.08	1.80	1.79	2.36	7.87	3.15	7.92	3.26	7.92	3.47	7.57	3.20
FeO	3.40	3.27	0.77	4.36	3.92	3.75	2.85	3.15	2.93	5.16	4.53	2.15	3.39	4.31	5.69	2.48	n.d.	n.d.	n.d.	n.d.	n.d.	n.d.	n.d.	n.d.
MnO	0.12	0.13	0.05	0.12	0.12	0.12	0.11	0.09	0.12	0.16	0.12	0.09	0.12	0.12	0.13	0.09	0.1	0.0	0.1	0.1	0.14	0.07	0.14	0.05
MgO	5.40	1.79	0.40	1.24	1.50	1.76	0.93	1.08	1.40	1.51	1.49	0.91	1.50	1.32	2.84	1.07	1.2	1.4	1.2	1.5	1.13	1.31	1.01	0.83
CaO	7.33	4.57	0.68	3.35	4.02	4.07	2.90	2.78	3.82	4.84	4.24	2.73	3.94	3.59	5.88	2.87	3.6	1.4	3.7	1.4	3.78	1.30	3.54	1.29
Na_2O	3.50	3.85	1.50	3.56	4.34	4.64	3.83	4.67	4.99	4.07	5.24	3.36	3.94	4.59	4.25	4.31	4.0	2.1	3.8	2.0	4.03	2.08	3.59	2.19
K_2O	1.44	1.96	6.07	2.79	2.28	2.63	3.16	3.35	2.44	3.02	2.83	5.57	3.03	2.82	2.13	3.89	2.6	4.7	2.9	4.5	2.93	4.96	3.41	5.32
P_2O_5	0.28	0.47	0.02	0.28	0.50	0.52	0.22	0.20	0.35	0.41	0.37	0.20	0.29	0.34	0.37	0.23	0.3	0.0	0.3	0.0	0.33	0.04	0.30	0.04
H_2O^+	n.d.	2.29	n.d.	4.00	1.57	1.25	3.08	1.11	1.31	2.32	1.55	1.81	2.48	2.15	1.93	2.11	3.3	5.9	2.9	6.0	2.2	4.7	3.0	4.8
H_2O^-	n.d.	0.59	n.d.	n.d.	0.44	0.68	0.27	0.15	0.22	0.51	0.15	0.53	0.52	0.10	n.d.	0.16	n.d.	n.d.	n.d.	n.d.	n.d.	n.d.	n.d.	n.d.
CO_2	n.d.	0.00	n.d.	n.d.	0.00	0.03	0.00	0.17	0.00	0.00	0.00	0.00	0.36	0.00	n.d.	0.00	n.d.	n.d.	n.d.	n.d.	n.d.	n.d.	n.d.	n.d.
Total	97.44	98.43	98.02	97.30	98.58	99.85	98.03	99.19	100.23	101.41	100.51	99.74	98.03	99.10	99.54	99.56	99.61	99.52	100.26	100.13	100.29	100.68	100.12	100.29
Volatile-free normalized values																								
SiO2	56.5	61.6	75.3	64.6	61.6	62.1	65.1	65.9	62.8	60.9	61.6	65.6	64.6	63.2	58.4	65.6	63.2	71.3	62.9	71.0	63.1	70.9	64.4	71.5
Σ alkalis	5.1	6.1	7.7	6.8	6.8	7.4	7.4	8.2	7.5	7.2	8.2	9.2	7.4	7.7	6.5	8.4	6.8	7.2	6.9	6.9	7.1	7.3	7.2	7.9

Analyses performed by ICP-AES by G.J. Aguirre-Díaz at the Geochemical Laboratory of the Department of Geological Sciences at the University of Texas at Austin, except those marked with asterisk, which were performed using XRF technique by Stephen Nelson at Tulane University (samples AM-39a, Am-258w) and by R. Lozano in the Institute for Geology of the Autonomous National University of Mexico. H_2O^+ determination was done by the Penfield method, and CO_2 by the acid evolution gravimetric method. Samples designated Es used loss of ignition values as H_2O^+. FeO was determined titrimetrically using Wilson's method. In XRF analyses FeO*=total iron volved sample digestion with HCl and HF, followed by repeated evaporation and solution in diluted HCl. This solution was filtered to collect the phases resistant to acid attack (e.g., zircon, apatite). The filtrate was dried and ignited at 800°C. The ignited sample was fused with NaOH in a nickel crucible. This material was dissolved and added to the filtered solution. The rare earth elements were separated by means of ion-exchange columns using a Dowex-80 resin. The elute containing the rare earths was preconcentrated by evaporation and the remaining salt brought back to solution in HNO_3. ICP-MS analysis used the standard sample digestion technique and sample instrumentation in a VG ICP-MS particularly calibrated for the lanthanides. For XRF, the major elements were analyzed using the standard procedure of fused pellets by means of a Fluxy burner and platinum crucibles, and for the rare earth elements pressed pellets were prepared by means of a digitally controlled press at 30 tons for 30 s.

Glass analyses were performed with a Jeol 733 electron microprobe in the Department of Geological Sciences, University of Texas at Austin. Glass analyses were done using a 15 KeV accelerating voltage, a beam current of 12 nA (on Faraday cup), and counting times of 20 s for both standards and unknowns. Na was analyzed first to reduce Na loss. The electron beam was rastered at a magnification of 32,000 with a minimum beam diameter across a square area 5–10 µm on an edge (Turbeville 1992). Several tests with standards were made to confirm that the probe raster mode provided more accurate values and better avoided Na loss than using a fixed unfocused beam for glass analyses.

Results

Major element and rare earth element data are given in Tables 2 and 3, and selected microprobe glass compositions of the Amealco ignimbrites are shown in Table 4. (The complete set of microprobe analyses shown in the following plots are available from the author as worksheet files via electronic mail.)

Na_2O loss and K_2O enrichment in glasses

It has been shown that silicic glasses can change their original alkali contents during hydration and devitrification (Lipman 1965; Noble 1970; Conrad 1984). Loss of Na and the concomitant enrichment of K is the common case for hydrated and devitrified glasses. In the Amealco ignimbrites, the glasses analyzed are mostly non-devitrified, but they are moderately hydrated, with total H_2O wt.% values up to 6, but in general within the 1–3 wt.% range (Table 2). As seen in Table 2, most of the volatile content is taken by the H_2O^+; thus, it can be assumed that the value for loss of ignition in the few samples where water was not analyzed (XRF analyses) is by far the most abundant volatile of the sample.

The effect of total water content in Na_2O and K_2O is shown in Fig. 6. The plots of H_2O wt.% (total water) vs Na_2O wt.% and H_2O wt.% vs K_2O wt.% show a tendency of depletion in Na_2O and enrichment in K_2O with increasing amounts of water in the sample (Fig. 6A, B). For instance, Na_2O changes from approximately 5 wt.% at 1 wt.% of H_2O to values around 2 wt.% at 6 wt.% H_2O (Fig. 6A). K_2O shows more scatter with respect to H_2O, but there is a tendency from approximately 2–3 wt.% at H_2O=1 wt.% to 4–5 wt.% at H_2O=6 wt.% (Fig. 6B).

The plot Na_2O–K_2O (Fig. 6C) shows the combined effect of Na_2O loss–K_2O enrichment, with the highest K_2O values corresponding to the lowest Na_2O values, and vice versa. This change accounts for a total of approximately 4 wt.% in Na_2O, and a total of approximately 3 wt.% in K_2O. In the same plot there are also shown the values on a dry basis (normalized volatile-free). Comparing the tendencies of the "wet" and the "dry" values, a small difference is observed among them, particularly for the water-rich values. The effect of Na_2O loss and K_2O enrichment is further reduced when it is used the total alkali–silica plot, because as one component increases, the other decreases in approximately the same proportion. This was confirmed by doing plots using both wet and dry sets; thus, following the common usage for presenting data, normalized volatile-free values were used in all figures.

Table 3 Rare earth element analyses of pumices in Amealco ignimbrites

Ignimbrite Sample	Zero Am-39	I Am-35	II Am-22	III Am-255	III Es1-b	III Es2-b	III Es4-b
La	17	28	34	41	27	24	28
Ce	40	64	72	76	85	89	70
Pr	8	n.d.	9	11	7	6	7
Nd	22	30	37	38	31	27	33
Sm	4	7	7	8	7	6	7
Eu	2	2	2	2	1.1	0.8	0.8
Gd	5	n.d.	7	7	7.4	6.5	7.7
Tb	0.6	1.2	1.2	1.3	1.1	1.0	1.0
Dy	4.4	n.d.	6.6	6.1	7.4	6.8	8.1
Ho	0.8	n.d.	1.1	1.1	1.2	1.1	1.3
Er	2.4	n.d.	3.4	2.8	4.2	4.0	4.6
Tm	0.2	n.d.	0.3	0.3	0.5	0.5	0.3
Yb	2.1	3.2	3.3	2.1	n.d.	n.d.	n.d.
Lu	0.3	0.5	0.5	0.2	0.5	0.5	0.4

Analyses done using ICP-AES and ion exchange by G. J. Aguirre-Díaz at the Geochemical Laboratory of the Department of Geological Sciences at the University of Texas at Austin, except ES series, which were performed using ICP-MS technique by O. Morton Bermea in the Institute for Geophysics of the Autonomous National University of Mexico

Table 4 Microprobe glass analyses of Amealco Tuff ignimbrites. *FeO** total iron calculated as FeO; *EH* Epitacio Huerta (at 13 km to the west)

Ignimbrite	I		I		II			II			III		
Site	EH		EH		EH			EH			EH		
Sample	Am-1		Am-36b		Am-22–3			Am-22–2			Am-20		
Analysis	5	13	21	44	31	35	36	1′	2	4′	6	31	49
SiO_2	67.4	71.1	63.4	61.6	67.7	66.7	71.2	71.6	66.0	62.5	66.3	71.9	57.7
TiO_2	0.26	0.28	0.96	1.33	0.40	0.52	0.37	0.21	0.46	0.94	0.50	0.39	1.06
Al_2O_3	13.5	14.2	16.4	15.3	13.6	14.7	13.6	13.1	15.5	14.4	14.8	14.4	8.9
FeO*	3.89	1.50	4.69	9.00	2.91	3.36	0.97	0.68	3.65	6.89	3.40	1.44	12.92
MnO	0.10	0.00	0.03	0.05	0.09	0.07	0.04	0.03	0.09	0.12	0.08	0.00	0.30
MgO	0.25	0.08	1.23	0.95	0.49	0.56	0.18	0.06	0.34	1.03	0.69	0.02	7.27
CaO	1.52	0.84	3.68	3.44	1.52	2.04	0.78	0.73	3.35	3.93	2.50	1.09	3.86
Na_2O	4.51	4.35	5.92	5.15	2.28	3.43	2.75	1.66	4.24	3.22	3.32	3.92	1.02
K_2O	4.31	4.32	1.65	2.28	6.80	5.40	6.40	7.42	3.94	3.75	4.67	5.49	2.26
P_2O_5	0.15	0.03	0.33	0.29	0.07	0.13	0.03	0.03	0.17	0.33	0.09	0.00	0.25
Total	95.9	96.7	98.3	99.4	95.9	97.0	96.4	95.5	97.7	97.0	96.4	98.7	95.5

Ignimbrite	II			III			II		III				
Site	Distal north			Proximal east			Distal west		25 km northeast				
Sample	Am-147			Am-171			Am-277		Am-77			Am-77 banded	
Analysis	1	3	6	7	9	13	1	11	1	18	41	30	28
SiO_2	73.9	63.4	61.5	62.6	71.8	67.4	60.4	65.2	66.2	64.2	62.9	60.5	69.4
TiO_2	0.21	0.84	0.99	0.27	0.56	0.53	1.07	0.85	0.47	0.79	0.78	0.85	0.26
Al_2O_3	12.2	14.5	14.3	16.9	15.8	14.1	15.5	15.5	14.3	14.8	14.7	14.7	13.7
FeO*	1.82	6.16	6.45	2.37	0.66	3.25	5.97	4.68	4.14	4.23	4.67	5.51	0.91
MnO	0.02	0.14	0.12	0.00	0.00	0.06	0.17	0.09	0.10	0.06	0.11	0.18	0.04
MgO	0.02	0.99	1.09	0.43	0.00	0.50	1.79	1.06	0.52	0.60	1.06	1.25	0.14
CaO	0.73	3.93	3.75	3.37	1.55	1.39	4.39	3.01	2.10	2.34	2.75	2.93	0.79
Na_2O	2.62	2.88	2.57	4.65	5.87	4.15	3.05	3.61	4.03	4.07	3.55	3.42	3.32
K_2O	5.04	3.86	4.19	3.01	2.18	4.59	3.01	3.14	3.30	3.60	3.99	4.35	5.67
P_2O_5	0.00	0.34	0.36	0.06	0.11	0.07	0.30	0.21	0.14	0.27	0.31	0.31	0.02
Total	96.6	97.0	95.3	93.7	98.5	96.0	95.6	97.4	95.3	95.0	94.8	94.0	94.2

Ignimbrite	III						III						
Site	40 km SW						30 km west						
Sample	Am-243a			Am-243a banded			Am-283			Am-283 banded			
Analysis	25	26	28	1	2	5	1	3	17	26	30	35	38
SiO_2	63.9	70.9	74.6	63.5	70.7	68.5	70.4	65.4	60.7	61.9	63.4	68.9	69.1
TiO_2	0.83	0.18	0.02	0.88	0.16	0.84	0.29	0.72	0.99	0.89	0.84	0.29	0.20
Al_2O_3	14.3	12.0	11.9	14.3	12.8	14.4	13.9	15.1	15.4	15.4	15.0	13.6	14.0
FeO*	6.79	4.15	0.43	6.30	2.20	6.13	2.52	4.43	6.08	5.33	5.17	2.28	2.58
MnO	0.10	0.06	0.00	0.12	0.03	0.14	0.03	0.11	0.16	0.11	0.11	0.00	0.04
MgO	0.84	0.05	0.02	0.84	0.05	0.83	0.18	0.89	1.55	1.28	0.96	0.21	0.20
CaO	3.38	0.62	0.46	3.70	1.36	3.44	1.18	2.90	4.09	3.78	3.21	1.32	1.29
Na_2O	3.00	2.92	2.32	2.41	1.76	3.18	2.98	3.42	3.47	3.85	4.05	3.16	3.52
K_2O	3.08	4.12	5.24	3.01	5.39	2.99	5.02	3.47	3.17	3.03	3.18	5.53	4.09
P_2O_5	0.23	0.00	0.00	0.22	0.00	0.23	0.02	0.10	0.30	0.19	0.10	0.02	0.02
Total	96.4	95.0	95.0	95.3	94.4	100.7	96.5	96.5	95.9	95.8	96.1	95.2	95.0

Analyses performed by G.J. Aguirre-Díaz at the Department of Geological Sciences of the Universityof Texas at Austin using a Jeol 733 electron microprobe. All distances mentioned in Site row are from the center of the Amealco caldera. Banded glass refers to heterogeneous pumice fragments; all others are discrete fragments that include matrix shards and small homogeneous pumices

Whole-rock pumices

The Amealco ignimbrite pumices have predominantly trachyandesite–trachydacite and andesitic–dacitic compositions (Fig. 7). All whole-rock analyses were done on visually homogeneous pumices. Figure 7 shows the minimum compositional variation of pumices within each of the Amealco ignimbrites. A larger variation would be expected if more analyses had been done, particularly for Amealco Zero and Amealco II. Pumice compositions are different, even those that were collected from the same ignimbrite unit at outcrop scale. For instance, silica for

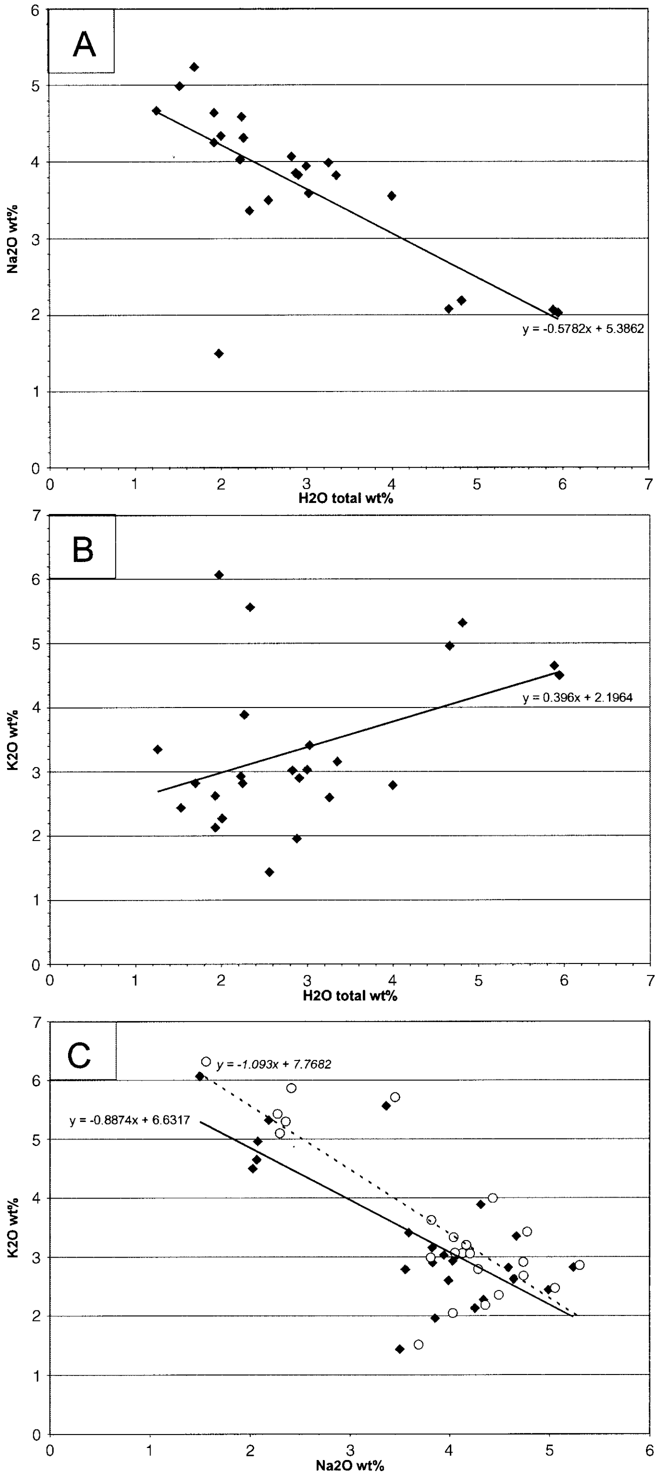

Fig. 6A–C The effect of total water content on Na_2O and K_2O contents of pumice samples of Amealco ignimbrites. Na_2O loss and K_2O enrichment are evident as water content increases in the pumices. All plots use non-normalized values of Table 2. **A** H_2O (total) wt.% vs Na_2O wt.% plot, showing the best fit line. **B** H_2O (total) wt.% vs K_2O wt.% plot, same explanation as in **A**. **C** Na_2O wt.% vs K_2O wt.% plot, showing that Na_2O contents reduce with increasing K_2O. For comparison, the normalized volatile-free values are also plotted. *Diamonds* non-normalized values; *circles* normalized values. Note similar tendency lines for both sets. See text for discussion

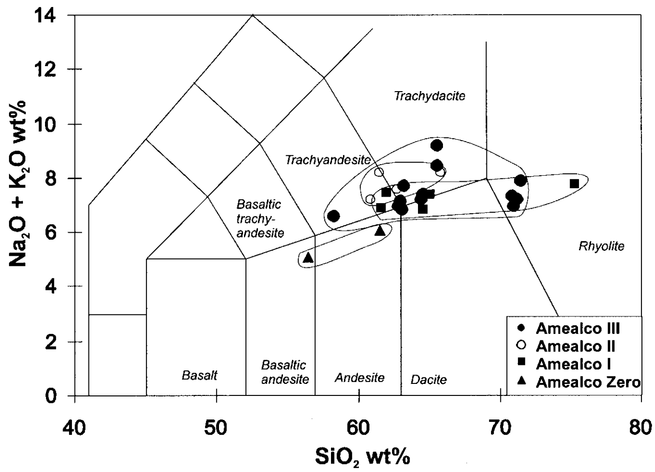

Fig. 7 Total alkali–silica plot (after Le Bas et al. 1986) of whole-rock pumice analyses of representative Amealco Tuff ignimbrites. Refer to Table 2 for data

Amealco I ranges between 61 and 75 wt.%; Amealco II, 60–66 wt.%; and Amealco III, 58–71 wt.% (Fig. 7; Table 2). Amealco Zero yielded the most mafic pumice composition with silica at approximately 56 wt.%.

Chondrite-normalized rare earth patterns for pumices are plotted in Fig. 8. A progressive increase of light rare earth elements takes place with time in the black pumices, from Amealco Zero (SiO_2=56 wt.%) to Amealco III (SiO_2=65 wt.%). Except for Amealco Zero, which shows a positive Eu anomaly, the ignimbrites show a small negative Eu anomaly, which is more marked in the rhyolitic pumices (Es series). The most primitive of the samples is Am-39 from Amealco Zero.

Microprobe glass analyses

Within a small area of a thin section it was possible to obtain glass compositions with silica contents ranging from 64 to 76 wt.% (Fig. 9a; Table 4). Banded glasses show contrasting compositions. For instance, rhyolite occurs in sharp contact with trachydacite, with silica contents of 74–76 wt.% and 64–67 wt.%, respectively (Fig. 9b; Table 4). Banded pumice fragments contained in the same bulk ignimbrite sample display an equivalent range in composition to that obtained from discrete glass fragments (small pumices and shards; Fig. 10; Table 4); however, there is a compositional gap in the banded glasses, whereas discrete glass compositions are more continuous (Fig. 10). This is also observed in a silica vs number of analyses histogram (Fig. 11), where discrete glass compositions range at least from 64 to 74 wt.% SiO_2 in all three main units.

Amealco I ignimbrite is vertically zoned, with the highest concentratrion of rhyolitic pumices in the base and dacitic pumices at the top (Fig. 11A). The other two ignimbrites do not show zonation as clearly as Amealco I, but rather a wide distribution of silica compositions from base to top (Fig. 11B, C). Amealco III in particular

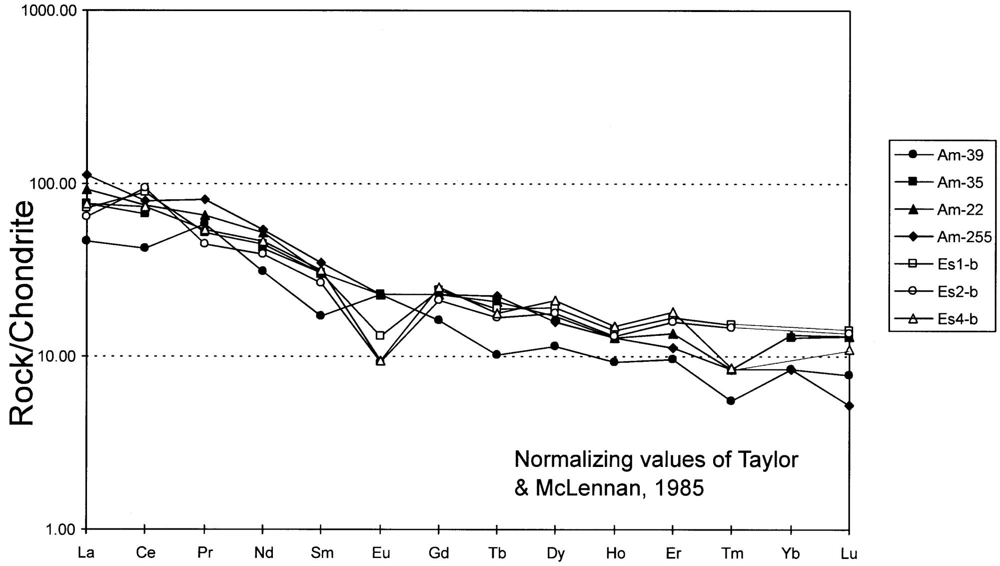

Fig. 8 Chondrite-normalized rare earth elements diagram of pumice samples of the Amealco ignimbrites. Note enrichment of the light rare earth elements with eruptive sequence. See Table 3 for non-normalized values. Amealco Zero: Ame-39; Amealco I: Am-35; Amealco II: Am-22; Amealco III: Am-255 and Es samples. All analyses from black pumices, except samples Es, which are from white pumices

shows the widest compositional range of all three, with a SiO_2 range of 60–77 (Fig. 11D).

Harker diagrams have different patterns for each ignimbrite (Fig. 12). Amealco I shows two clusters separated by a gap, each representing a magma in the subcaldera magma chamber. Amealco II concentrates most of the data in silica contents higher than 68, but still shows a couple of points as a separate group around SiO_2=65 wt.%. Most analyses of Amealco III are within the 64–73 SiO_2 range, but a single analysis has a more mafic composition at SiO_2 around 60. This single point may represent a volumetrically minor mafic magma in the subcaldera system. It has an MgO content of nearly 8 wt.% and total FeO of approximately 14 wt.%, which is much more mafic than the rest of the data in Amealco III ignimbrite (analysis 49, see Table 4) and any glass analysis in the three ignimbrites (Fig. 12). The most mafic of the major ignimbrites, as bulk tuff, is Amealco I. The other two are more evolved, with most of the data at silica values higher than 64 wt.% and with corresponding higher K_2O contents (Fig. 12). Minimum silica values shifted from Amealco I to Amealco II, and returned to less silica-rich values from Amealco II to Amealco III (Figs. 11, 12). There is also a marked increase of rhyodacitic glass compositions (SiO_2=68–72) from Amealco I to Amealco II. Although Amealco III shows in general a continuous trend, several components have a tendency to become bimodal, such as TiO_2, CaO, K_2O, and P_2O_5 (Fig. 12), suggesting that the process was interrupted when Amealco III ignimbrite was erupted, possi-

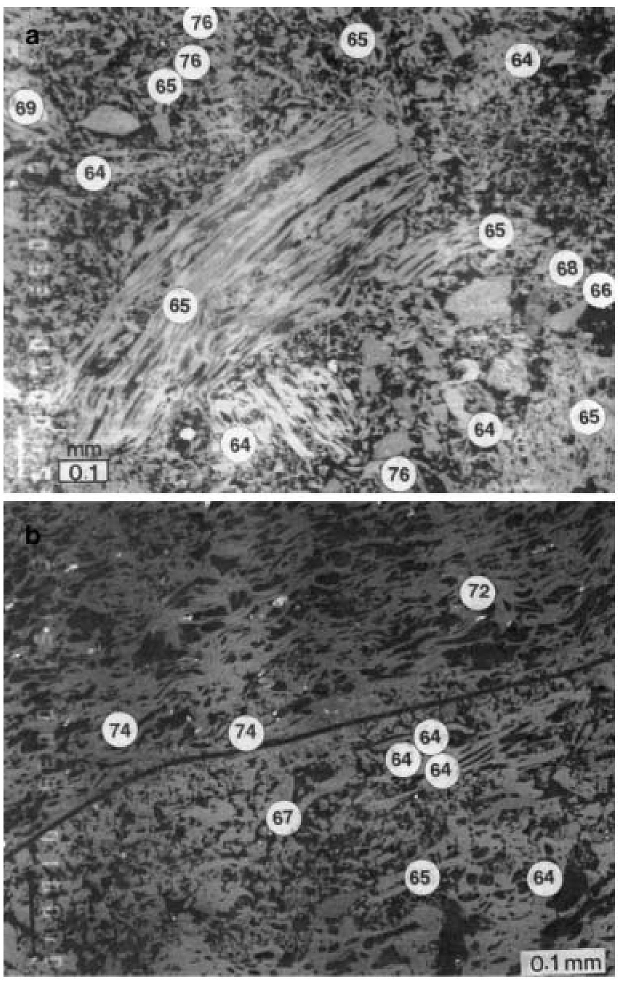

27 28 29

Fig. 9a, b Backscattered electron images of thin sections of Amealco ignimbrites. **a** Bulk ignimbrite (sample Am-147 of Table 4) showing discrete glasses (shards and small pumice fragments). *Circles* represent spot glass analyses by microprobe and *numbers* indicate the SiO_2 content (normalized volatile-free). Note the well-mingled character of pumice lumps and glass shards with silica contents of 64–76 wt.% coexisting in a small area. **b** Banded pumice (sample Am-77 of Table 4). Glass above the contact (*black line*) is rhyolite and glass below the contact is trachydacite. Note the sharp contact between the two glasses, indicating that the liquids did not have enough time to interact to produce a hybrid melt bly by an input of mafic magma, which triggered the eruption as is explained below.

Although each ignimbrite spans a wide compositional range, in general K_2O (Fig. 12), SiO_2 (Fig. 11), the light rare earth elements (Fig. 8), and the bulk tuff crystal content (Fig. 5) show a moderate increase with time, from Amealco I to Amealco II to Amealco III, suggesting that magmas in the subcaldera magma chamber became more evolved from the first erupted ignimbrite to the last. This is further confirmed if the small Amealco Zero is also considered, because this is the ignimbrite with the most primitive compositions (Figs. 7, 8).

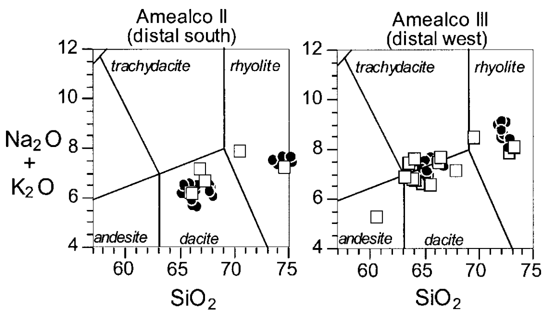

Fig. 10 Total alkali–silica diagrams (Le Bas et al. 1986) for glasses of two Amealco Tuff ignimbrite samples, one from a southern locality (Am-243; Table 4) and the other from a western site (Am-283; Table 4). The plots show banded (*circles*) and discrete (*squares*) glasses of each sample, where banded glass compositions were obtained from a single heterogeneous pumice fragment, and discrete glass compositions were obtained from matrix shards and small homogeneous pumice fragments. In both examples banded pumices and discrete glasses are contained in the same hand-size bulk tuff collection

Discussion

Field and laboratory observations in the Amealco ignimbrites have shown that: (a) the different glass populations are juvenile; (b) the glasses are well mingled, even at the microscopic scale (tuff matrix or individual shards); (c) all of the aforementioned features are observed in all three major Amealco ignimbrites; (d) each ignimbrite represents a discrete eruptive episode that is separated by thin (<0.2 m thick) lake deposits, paleosols, or irregular, reworked paleo-surfaces; and (e) banded pumice lumps occur in all ignimbrites.

These observations suggest that: (a) mingling of magmas occurred simultaneously to the eruption of the pyroclastic flows that formed the Amealco Tuff ignimbrites; (b) the different melts were simultaneously ejected; and (c) the magmatic and volcanic processes that caused the magma mingling occurred at least three times to produce three ignimbrites composed of mingled glasses.

Based on the different whole-rock pumice compositions observed in the Amealco ignimbrites, the magma chamber apparently contained magmas with composi-

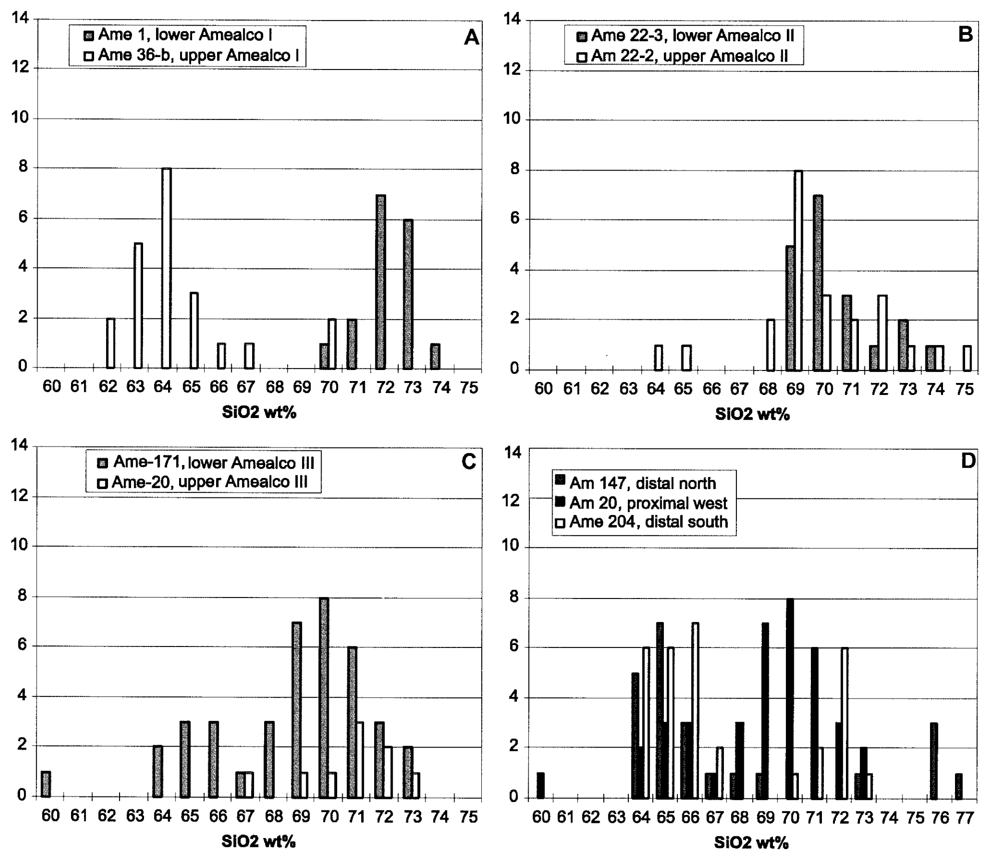

Fig. 11A–D Histograms of wt.% SiO_2 (normalized volatile-free) vs number of analyses of glass shards and small pumice fragments, showing the distribution of compositions in all three Amealco ignimbrites at the type locality of Epitacio Huerta shown in Fig. 2 (except **D** and sample Am-171, which is from lower Amealco III ignimbrite collected a few kilometers to the east). Note that each ignimbrite spans a range in silica contents of over 10%. **A** Amealco I shows a bimodal distribution, **B** Amealco II a more nearly normal distribution, and **C** Amealco III a poorly developed bimodal distribution. **D** Histogram of Amealco III ignimbrite, obtained from several samples collected at different sites, proximal and distal. SiO_2 ranges from 60 to 77 wt.%, with most data between 64 and 73 wt.%

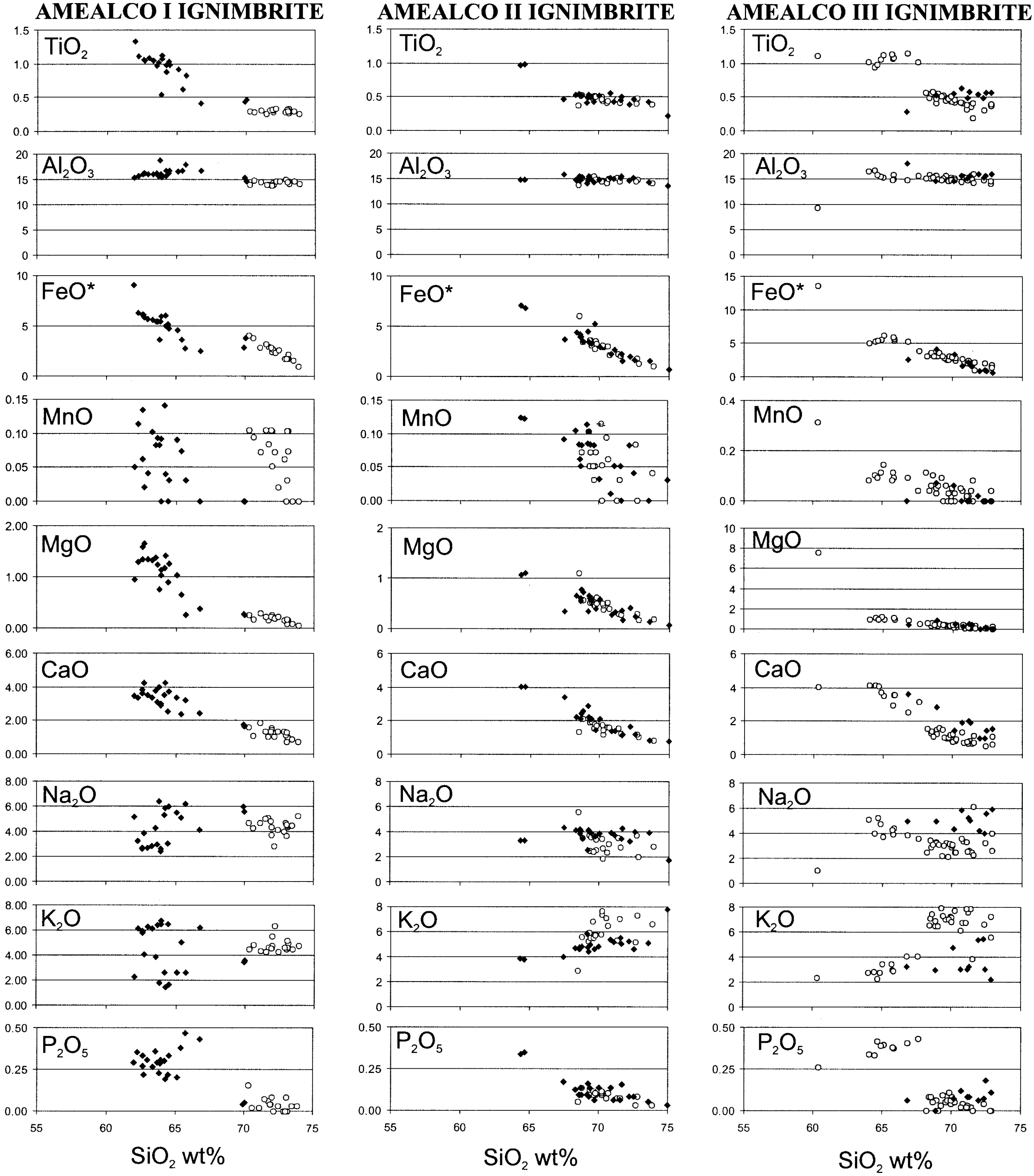

Fig. 12 Harker variation diagrams of glass shards and small pumice fragments of three representative samples of the Amealco Tuff ignimbrites at Epitacio Huerta site (Figs. 1, 2). *Circles* sample from the base of the ignimbrite; *diamonds* sample from the upper portion of the ignimbrite. Same samples as in Fig. 11

tions from andesitic–trachyandesitic to dacitic–trachydacitic to rhyolitic, before each explosive eruption that produced these ignimbrites. The geometry of this heterogeneity is unknown. It may have been either as vertical concentric zones produced by sidewall crystallization or by non-concentric horizontal layering. Studying the glass compositions of the ignimbrites in the most thoroughly studied measured section, at Epitacio Huerta (Fig. 2), it

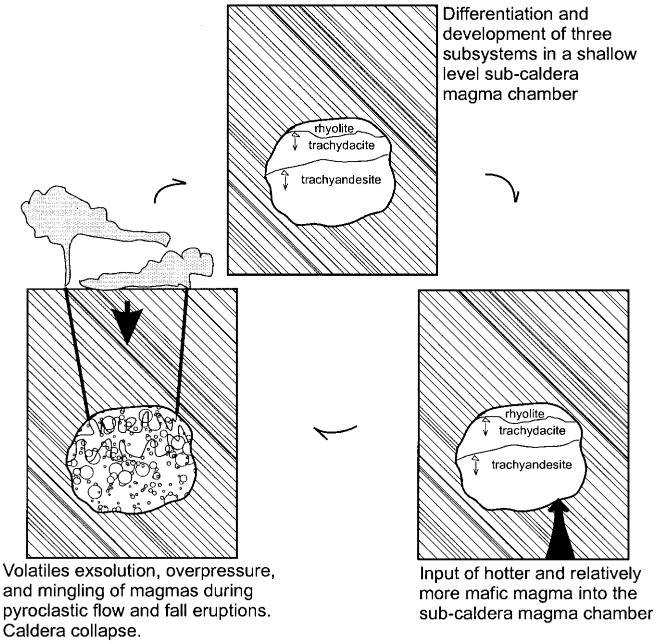

Fig. 13 Schematic model of the inferred process that caused repetitive mingling of magmas that produced the Amealco Tuff ignimbrites. The process starts with differentiation of a subcaldera magma chamber, forming a vertically zoned magma chamber with trachyandesite, trachydacite, and rhyolite layered magmas. The magma chamber receives an input of a hotter magma, possibly with a basaltic–andesite composition (Am-39 sample; Table 2). This input causes an increase of temperature in the magma chamber, which in turn causes convection, volatile exsolution, and mingling of the differentiated magmas. At the same time, the overpressure caused by the volatile exsolution produced the explosive eruption of the mingled magmas and caldera collapse. After eruption, the remaining magmas start to reestablish equilibrium conditions within the magma chamber, and start a new cycle

is observed that Amealco I shows a bimodal distribution with peaks at SiO_2=64 wt.% and at SiO_2=72 wt.% (Fig. 11). This suggests the presence of at least two magmas (a low SiO_2 dacite and a low SiO_2 rhyolite) in the subcaldera magma chamber prior to eruption of Amealco I ignimbrite. Amealco II ignimbrite shows a single peak at SiO_2=69 wt.% with an asymmetric normal distribution (Fig. 11), suggesting that the two magmas mentioned previously for Amealco I hybridized to form the magma represented in Amealco II. This observation is confirmed by the Harker diagrams (Fig. 12). At the time when Amealco III was erupted, apparently the magmas in the subcaldera magma chamber were reestablishing zonation similar to that when Amealco I erupted. This is observed in the histogram of Amealco III, which shows a poorly developed bimodal distribution with peaks at SiO_2=65 wt.% and 70 wt.%, and in the patterns of the Harker diagrams, particularly for TiO_2, CaO, K_2O, and P_2O_5 (Fig. 12). The differentiation mechanism was probably crystal fractionation, as bulk crystal content increases from Amealco I to Amealco III (Fig. 5).

There are several models proposed for mingling of magmas and simultaneous tapping of the mingled magmas (e.g. Sparks et al. 1977; Koyaguchi 1985; Blake and Campbell 1986; Blake and Ivey 1986; Pallister et al. 1991, 1996; Freundt and Schmincke 1992; Thomas et al. 1993). Following the basic model proposed by Sparks et al. (1977), it is suggested that the magma chamber beneath Amealco caldera received an input of hotter, less evolved, and relatively more mafic magma than the magma chamber into its base (Fig. 13). Representatives of this mafic magma in the Amealco case may be sample Am-39a (Table 2), a highly vesiculated scoria lump with a basaltic andesite composition within Amealco Zero ignimbrite, and the andesitic glass with MgO=7.3 wt.% and FeO*=13 wt.% (Amealco III, glass 49, EH site; Table 4) observed in Amealco III ignimbrite. This magma input caused volatile exsolution, overpressure, and explosive eruption of mingled magmas. Mingling of magmas could have started just after the input of the mafic magma, by the upward motion of gas bubbles during the exsolution of volatiles, as Thomas et al. (1993) explain in their experimental model. This was immediately followed by the explosive eruptions of mingled magmas, and caldera collapse. The collapsing blocks into the upper part of the magma chamber may have contributed to the mingling of magmas during the climactic eruptions.

With such a model the following features observed in the Amealco ignimbrites can be explained: (a) the occurrence of several glass populations with an overall range in composition (a magma zone for each population); (b) insufficient time for the distinct magmas to homogenize, as each zone was a subsystem within the magma chamber that became mingled during eruption; (c) the explosive eruption, caused by overpressure due to exsolution of volatiles; and (d) occurrence of the three ignimbrites Amealco I, Amealco II, and Amealco III, each with evidence of magma mingling.

It is unlikely that the entire magma chamber would be emptied in any ignimbrite eruption, so a large mass of mingled magma would remain in the chamber. Repetition of such cycles as the one shown in Fig. 13 should lead to changes in liquid composition. This suggests progressive changing of the remaining liquids in the subcaldera magma chamber as the Amealco ignimbrites were formed. These changes are shown by chondrite-normalized rare earth element plots for representative samples of the Amealco ignimbrites (Fig. 8). A progressive increase in the light rare earth elements from Amealco Zero to Amealco III is evident in the black pumices, which is accompanied with an increase in the alkalis (Fig. 7), K_2O (Fig. 12), and the general shift of the minimum and maximum contents of SiO_2 to higher values (Fig. 11). Crystal assemblages remained the same in all four ignimbrites, with plagioclase>hypersthene>augite>Fe–Ti oxides±apatite±olivine, with olivine being relatively more abundant in Amealco Zero ignimbrite (<2 vol.%, compared with <1 vol.% in the major ignimbrites). However, bulk crystal content increased markedly from Amealco I to Amealco III (Fig. 5); thus, the remaining magma after the end of each cycle, as shown in

Fig. 13, became more evolved with respect to the previous one.

The deposits between the major ignimbrites indicate pauses in the volcanic activity. The duration of these relatively quiescent periods is still unknown. The intervals were long enough for the magma chamber to become vertically or concentrically zoned before the subsequent input of new magma took place, triggering the mingling of magmas and the associated explosive eruption.

Conclusion

The following conclusions were reached as a result of this study:

1. The Amealco ignimbrites are composed mainly of mingled glass fragments with different compositions, both at the shard and pumice lump scales. Whole-rock pumice compositions range from basaltic andesite (SiO_2=56 wt.%) to rhyolite (SiO_2=75 wt.%), and microprobe analyses of shards and small pumices range from andesite (SiO_2=61 wt.%) to high-silica rhyolite (SiO_2=75 wt.%) within the a single ignimbrite.
2. Individual ignimbrites contain distinct glass compositions dispersed throughout the deposit.
3. The mechanism that produced each of these ignimbrites was repeated at least three times in separate events from the same source, the Amealco caldera. The model proposed here consists of a zoned magma chamber that receives input of hotter magma. This triggers gas exsolution, mingling of magmas, overpressure, and finally an explosive eruption of the mingled melts as pyroclastic flows and fallouts.

Acknowledgements This work was greatly improved by the comments of F.W. McDowell, B.N. Turbeville, R. Lange, J. Luhr, M. Dungan, M. Streck, M.L. Coombs, and particularly W. Hildreth, on previous versions of the paper. Special thanks to D.S. Barker for his great help and contribution to this paper. I also thank for the ICP-MS analyses performed by Ofelia Morton of Instituto de Geofísica, UNAM, and the XRF analyses performed by Stephen Nelson of Tulane University, and by Rufino Lozano of Instituto de Geología, UNAM. This work was supported in part by the Geology Foundation of the Department of Geological Sciences of the University of Texas at Austin, a research grant from the Geological Society of America, a scholarship from the Dirección General de Asuntos del Personal Académico, UNAM, and grants from the Dirección General de Asuntos del Personal Académico PAPIIT-IN-106594; PAPIIT-IN-120999.

References

Aguirre-Díaz GJ (1993) The Amealco caldera, Queretaro, Mexico: geology, geochronology, geochemistry, and comparison with other silicic centers of the Mexican Volcanic Belt. PhD dissertation, Univ Texas, Austin, Texas, 401 pp

Aguirre-Díaz GJ (1996) Volcanic stratigraphy of the Amealco caldera and vicinity, central Mexican Volcanic Belt. Rev Mexicana de Ciencias Geológicas, Instituto de Geología, UNAM 13: 10–51

Aguirre-Díaz GJ, Urrutia-Fucugauchi J, Soler-Arechalde AM (2000) Stratigraphy, K-Ar ages, and magneto-stratigraphy of the Acambay graben, central Mexican Volcanic Belt. In: Delgado-Granados H, Aguirre-Díaz GJ, Stock J (eds) Cenozoic Tectonics and Volcanism of Mexico. Geol Soc Amer Spec Pap 334:179–193

Bardintzeff JM (1992) Magma mixing processes in volcanic contexts, a thermodynamic approach with the examples of St. Vincent Soufriere volcano, West Indies and Cerro Chiquito, Guatemala. Terra Nova 4:553–566

Blake S, Campbell IH (1986) The dynamics of magma-mixing during flow in volcanic conduits. Contrib Mineral Petrol 94:72–81

Blake S, Ivey GN (1986) Magma-mixing and the dynamics of withdrawal from stratified reservoirs. J Volcanol Geotherm Res 27:153–178

Briggs RM, Gifford NG, Moyle MR, Taylor SR, Norman MD, Houghton BF, Wilson CJN (1993) Geochemical zoning and eruptive mixing in ignimbrites from Mangakino volcano, Taupo Volcanic Zone, New Zealand. J Volcanol Geotherm Res 56:175–203

Conrad WK (1984) The mineralogy and petrology of compositionally zoned ash flow tuffs, and related silicic volcanic rocks, from the McDermitt caldera complex, Nevada–Oregon. J Geophys Res 89:8639–8664

Freundt A, Schmincke HU (1992) Mixing of rhyolite, trachyte and basalt magma erupted from a vertically and laterally zoned reservoir, composite flow P1, Gran Canaria. Contrib Mineral Petrol 112:1–19

Fries C Jr, Ross CS, Obregón A (1977) Mezcla de vidrios en los derrames cineríticos Las Américas de la región de El Oro-Tlalpujahua, Estados de México y Michoacán, parte centro-meridional de México. Boletín Instituto Geología Universidad Nacional Autónoma de México 70:1–84 (in Spanish)

Koyaguchi T (1985) Magma mixing in a conduit. J Volcanol Geotherm Res 25:365–369

Le Bas MJ, Le Maitre RW, Streckeisen A, Zanettin B (1986) A chemical classification of volcanic rocks based on the Total Alkali-Silica system. J Petrol 27:745–750

Lipman PW (1965) Chemical comparison of glassy and crystalline volcanic rocks. Bull US Geol Surv 1201-D

Lipman PW (1967) Mineral and chemical variations within an ash-flow sheet from Aso caldera, southwestern Japan. Contrib Mineral Petrol 16:300–327

Mahood GA, Gilbert CM, Carmichael ISE (1985) Peralkaline and metaluminous mixed-liquid ignimbrites of the Guadalajara region, Mexico. J Volcanol Geotherm Res 25:259–271

Mandeville CW, Carey S, Sigurdsson H (1996) Magma mixing, fractional crystallization and volatile degassing during the 1883 eruption of Krakatau volcano, Indonesia. J Volcanol Geotherm Res 74:243–274

Martin RC, Lewis JF (1963) Nature of glass in New Zealand ignimbrites. Nature 197:1166–1167

Nixon GT (1982) The relationship between Quaternary volcanism in central Mexico and the seismicity and structure of subducted ocean lithosphere. Geol Soc Am Bull 93:514–523

Noble DC (1970) Loss of sodium from crystallized comendite welded tuffs of the Miocene Grouse canyon member of the Belted Range tuff, Nevada. Bull Geol Soc Am 81:2677–2688

Orsi G, Civetta L, D'Antonio M, Girolamo P di, Piochi M (1995) Step-filling and development of a three-layer magma chamber: the Neapolitan Yellow Tuff case history. J Volcanol Geotherm Res 67:291–312

Pallister JS, Hoblitt RP, Reyes AG (1991) A basalt trigger for the 1991 eruptions of Pinatubo volcano? Nature 356:426–428

Pallister JS, Hoblitt RP, Meeker GP, Knight RJ, Siems DF (1996) Magma mixing at Mount Pinatubo: petrographic and chemical evidence from the 1991 deposits. In: Newhall CG, Punongbayan R (eds) Fire and mud: eruptions of Mount Pinatubo, Philippines. Quezon City, Philippine Institute of Volcanology and Seismology. University of Washington Press, Seattle, pp 687–731

Pardo M, Suárez G (1995) Shape of the subducted Rivera and Cocos plates in southern Mexico: seismic and tectonic implications. J Geophys Res 100:357–373

Sparks RSJ, Self S, Walker GPL (1973) Products of ignimbrite eruptions. Geology 1:115–118

Sparks RSJ, Sigurdsson H, Wilson L (1977) Magma mixing: a mechanism for triggering acid explosive eruptions. Nature 267:315–318

Streck MJ, Grunder AL (1997) Compositional gradients and gaps in high-silica rhyolites of the Rattlesnake Tuff, Oregon. J Petrol 38:133–163

Streck MJ, Grunder AL (1999) Enrichment of basalt and mixing of dacite in the rootzone of a large rhyolite chamber: inclusions and pumices from the Rattlesnake Tuff, Oregon. Contrib Mineral Petrol 136:193–212

Taylor SR, McLennan SM (1985) The continental crust: its composition and evolution. Blackwell, Oxford

Thomas N, Tait S, Koyaguchi T (1993) Mixing of stratified liquids by the motion of gas bubbles: application to magma mixing. Earth Planet Sci Lett 115:161–175

Turbeville BN (1992) Relationships between chamber margin accumulates and pore liquids: evidence from arrested in situ processes in ejecta, Latera caldera, Italy. Contrib Mineral Petrol 110:429–441

Walker GPL, Skelhorn RR (1966) Some associations of acid and basic igneous rocks. Earth Sci Rev 2:93–109

Williams H (1952) Volcanic history of the Meseta Central Occidental, Costa Rica. California. Univ Publ Geol Sci 29:145–180